Research Square

Preprints are preliminary reports that have not undergone peer review.
They should not be considered conclusive, used to inform clinical practice,
or referenced by the media as validated information.

Translating Perivascular Inflammation Imaging into Precision Coronary Care: An Ex plainable Nomogram Integrating Pericoronary Adipose Tissue Attenuation Index with Anatomical and Functional CT Biomarkers for Acute Coronary Syndrome Discrimination

yinlong qi
Shanghai Fengxian District Traditional Chinese Medicine Hospital
Haiyang Zhang
Shanghai Fengxian District Traditional Chinese Medicine Hospital
YaNan Li
Shanghai Fengxian District Traditional Chinese Medicine Hospital
Ting Ni
Shanghai Fengxian District Traditional Chinese Medicine Hospital
Sheng Zhou
fortify2008@163.com
Shanghai Fengxian District Traditional Chinese Medicine Hospital
JinJun Dong
Shanghai Fengxian District Traditional Chinese Medicine Hospital
Mingzhu Yu
Shanghai Fengxian District Traditional Chinese Medicine Hospital
Xin Liu
Shanghai Fengxian District Traditional Chinese Medicine Hospital

Research Article

Keywords:

Posted Date: November 14th, 2026

DOI: https://doi.org/10.21203/rs.3.rs-11139418/v1

License: This work is licensed under a Creative Commons Attribution 4.0 International License.
Read Full License

Additional Declarations:
No competing interests reported.

Tables are available in the Supplementary Files section.

Translating Perivascular Inflammation Imaging into Precision Coronary Care: An Explainable Nomogram Integrating Pericoronary Adipose Tissue Attenuation Index with Anatomical and Functional CT Biomarkers for Acute Coronary Syndrome Discrimination

Authors: Yinlong Qi[1], Haiyang Zhang[1], YaNan Li[1], Ting Ni[1], Sheng Zhou[1], JinJun Dong[1], Mingzhu Yu[1], Xin Liu[1]

Affiliations: [1]Department of Radiology, Shanghai Fengxian District Traditional Chinese Medicine Hospital, Shanghai 201400, China

Corresponding Author: Sheng Zhou, MD Department of Radiology Shanghai Fengxian District Traditional Chinese Medicine Hospital No. 9588 South Jiangchuan Road, Fengxian District, Shanghai 201400, China Email: fortify2008@163.com

Structured Abstract

Background: Acute coronary syndrome (ACS) and stable coronary artery disease (SCAD) present overlapping clinical phenotypes, yet mandate divergent therapeutic strategies—urgent revascularization versus pharmacological optimization. Current diagnostic reliance on high-sensitivity cardiac troponin dynamic monitoring introduces hazardous delays (4–6 hours detection window) and yields false negatives in 20% of non-ST-elevation myocardial infarction. Pericoronary adipose tissue attenuation index (FAI), quantifying vascular inflammation through computed tomography (CT) attenuation changes in pericoronary fat, offers mechanistic insight into coronary plaque destabilization. However, the translational pathway from this biomarker to clinically actionable decision support remains incompletely realized, particularly regarding integration with established anatomical and functional parameters and explicit clinical interpretability.

Hypothesis: A mechanistically grounded, multi-dimensional nomogram combining FAI with coronary CT angiography (CCTA)-derived anatomical stenosis (%DS), left ventricular ejection fraction (LVEF), and smoking status—rendered interpretable through SHapley Additive exPlanations (SHAP)—would achieve robust ACS-SCAD discrimination while providing transparent, auditable decision logic suitable for clinical implementation.

Methods: In this prospective diagnostic accuracy study adhering to TRIPOD 2019 guid elines, 388 patients (ACS 117 [30.2%], SCAD 271 [69.8%]) underwent CCTA with st andardized FAI, %DS, and LVEF acquisition. Stratified randomization (7:3) produced t raining (n=271) and validation (n=117) sets with preserved outcome distribution. Least absolute shrinkage and selection operator (LASSO) regression with 10-fold stratified c ross-validation compared lambda.min versus lambda.1se selection criteria, followed by multivariable logistic regression. Performance was assessed by area under the receiver operating characteristic curve (AUC), calibration, Brier score, and decision curve analy sis. KernelSHAP parsed individualized decision contributions. Regulatory-readiness was evaluated through predetermined change control documentation and explanation stabilit y assessment.

Results: LASSO lambda.min retained %DS, FAI, LVEF, RVEF, and smoking; lambda.1 se selected only %DS and FAI. Final model incorporated %DS, FAI, LVEF, and smok ing based on mechanistic non-overlap (RVEF-LVEF functional redundancy) and epidem iological importance. Multivariable analysis demonstrated %DS (OR 1.03, 95% CI: 1.0 1–1.04, $P < 0.001$) and FAI (OR 1.04, 95% CI: 1.02–1.06, $P < 0.001$) as positive A CS predictors; LVEF as protective (OR 0.96, 95% CI: 0.92–0.99, $P = 0.032$); smoking as marginally non-significant (OR 1.83, 95% CI: 0.87–3.86, $P = 0.110$) but increment ally contributory. Nomogram achieved AUC 0.86 (95% CI: 0.82–0.91) in training and 0.82 (95% CI: 0.75–0.90) in validation. Optimal cutoff 0.291 (Youden index) yielded t raining sensitivity 0.80, specificity 0.82, negative predictive value 0.91; validation sensi tivity 0.73, specificity 0.72, negative predictive value 0.83. Calibration was satisfactory (Hosmer-Lemeshow $P = 0.347$ and $P = 0.405$). Decision curve analysis demonstrated net benefit across threshold probability 0.10–0.55. SHAP analysis established a mecha nistic hierarchy: %DS and FAI as dominant drivers (mean |SHAP| 0.75 and 0.70), LV EF as a functional protective modifier (0.35), and smoking as a behavioral risk stratifi er (0.20). Individual force plots enabled case-level explanation with documented contri bution stability.

Conclusions: The %DS-FAI-LVEF-smoking nomogram achieves favorable ACS discrimi natory accuracy with acceptable generalization. SHAP-enhanced interpretability satisfies emerging transparency requirements for artificial intelligence-enabled medical devices,

supporting regulatory-ready clinical translation.

Translational Significance: This study bridges the critical T1–T2 translational gap by converting perivascular inflammation biology (FAI) into an evidence-based diagnostic tool validated for a specific clinical decision context. The "one-stop" CCTA acquisition strategy—yielding anatomical, inflammatory, and functional data from a single examination—addresses implementation barriers in time-critical emergency settings. Explicit SHAP-based explainability exceeds current "black box" machine learning limitations, aligning with FDA and EMA guidance on predetermined change control and transparency documentation for clinical artificial intelligence. These design elements collectively reduce translational friction from research prototype to prospective clinical trials and eventual regulatory approval, advancing precision coronary care through mechanism-informed, transparently interpretable decision support.

Keywords: Acute coronary syndrome; pericoronary adipose tissue attenuation index; coronary computed tomography angiography; translational medicine; explainable artificial intelligence; diagnostic nomogram; precision cardiovascular medicine; regulatory science

Introduction

The Clinical Imperative: ACS-SCAD Discrimination at the Translational Interface

Acute coronary syndrome (ACS)—encompassing ST-elevation myocardial infarction (STEMI), non-ST-elevation myocardial infarction (NSTEMI), and unstable angina—demands urgent therapeutic escalation, including revascularization and intensified antithrombotic therapy [1]. Conversely, stable coronary artery disease (SCAD) management prioritizes pharmacological optimization with elective invasive assessment [2]. This therapeutic divergence renders accurate discrimination a critical decision node; yet, clinical presentation overlap generates substantial diagnostic uncertainty, with emergency department misdiagnosis rates of 5%–10% and associated mortality escalation [3].

Contemporary diagnostic pathways rely predominantly on high-sensitivity cardiac troponin (hs-cTn) dynamic monitoring and electrocardiographic evolution. These modalities

harbor inherent limitations: the obligatory 4–6 hour detection window introduces therapeutic delay; micro-injury, renal insufficiency, and skeletal muscle pathology generate false positives; and approximately 20% of NSTEMI patients present with initially normal troponin values [4,5]. Traditional risk scores—Global Registry of Acute Coronary Events (GRACE) and Thrombolysis In Myocardial Infarction (TIMI)—were developed for prognostication rather than diagnostic discrimination, and notably omit imaging biomarkers [5]. This diagnostic gap represents a translational failure: validated pathophysiological mechanisms have not been converted into timely, actionable clinical tools.

Mechanistic Foundation: Perivascular Inflammation as a Theranostic Target

Coronary inflammation constitutes the unifying pathophysiological mechanism of plaque destabilization in ACS [6]. Pericoronary adipose tissue (PCAT)—the visceral fat depot encasing epicardial coronary arteries—lacks a fascial boundary with the vascular adventitia, permitting bidirectional paracrine signaling [7]. Inflammatory cytokines released from activated coronary plaques—tumor necrosis factor-α (TNF-α), interleukin-6 (IL-6), interleukin-1β (IL-1β)—diffuse into adjacent adipocytes, suppressing lipid accumulation and inducing phenotypic transformation toward smaller, less differentiated adipocytes with elevated CT attenuation [8]. This biological mechanism, initially characterized in preclinical models and subsequently validated through human histopathological studies, provides the mechanistic rationale for pericoronary adipose tissue attenuation index (FAI) as a non-invasive surrogate of coronary inflammation [9].

Oikonomou and colleagues pioneered FAI quantification, demonstrating prognostic value for major adverse cardiovascular events independent of luminal stenosis severity [10, 11]. FAI offers distinctive translational advantages: anatomical colocalization with target vessels enables lesion-specific assessment; dynamic response to anti-inflammatory therapy supports therapeutic monitoring; and seamless integration into standard CCTA protocols requires no additional radiation, contrast, or cost [12]. However, standalone FAI diagnostic accuracy remains modest (AUC approximately 0.75–0.80), and its specific value for ACS-SCAD differential diagnosis—distinct from prognostic prediction—remains insufficiently elucidated [13]. This represents a T1 translational gap: a mechanistically validated biomarker awaits optimization for a specific clinical decision context.

The Implementation Challenge: From Biomarker to Decision Support

Widespread deployment of machine learning in cardiovascular imaging has precipitated "black box" concerns, undermining clinician trust, regulatory approval, and clinical adoption [14]. The SHapley Additive exPlanations (SHAP) framework, grounded in cooperative game theory, assigns marginal contribution values to individual predictors, unifying global feature importance with individualized case explanation [15]. Critically, SHAP values represent statistical association estimates—"predictive relevance" rather than "causal effect"—a distinction that must be explicitly communicated to prevent mechanistic overinterpretation [16].

Regulatory agencies have responded with escalating transparency requirements. The U.S. Food and Drug Administration's 2021 Action Plan for Artificial Intelligence/Machine Learning-Based Software as a Medical Device emphasizes "predetermined change control plans" and "real-world performance monitoring" [17]. The European Medicines Agency's 2023 reflection paper mandates "sufficient interpretability" to enable "meaningful human oversight" [18]. These evolving standards create an implementation barrier for conventional machine learning models while simultaneously establishing a pathway for explicitly interpretable designs.

Study Objectives and Translational Framework

We employed a staged translational research framework aligning with the National Institutes of Health translational taxonomy [19]:

T1 translation (mechanism to candidate application): Validate FAI as an inflammation surrogate within ACS-SCAD diagnostic discrimination
T2 translation (candidate application to evidence-based guideline): Develop and internally validate a multi-dimensional nomogram with explicit interpretability
T3 preparation (guideline to practice): Design for regulatory-ready implementation through SHAP-based transparency and "one-stop" CCTA workflow integration

Specific objectives were: (1) to develop and validate an interpretable nomogram integrating %DS, FAI, LVEF, and smoking status for ACS versus SCAD differentiation; (2)

to systematically compare LASSO lambda selection criteria (lambda.min versus lambda.1se) for variable selection, balancing statistical parsimony with mechanistic completeness; and (3) to achieve transparent, auditable individualized decision explanation through the SHAP framework, with explicit documentation of regulatory-readiness elements.

Materials and Methods

Study Design and Ethics

This diagnostic model development and validation study adhered to the Declaration of Helsinki, the Ethical Review Measures for Biomedical Research Involving Human Subjects, and the Transparent Reporting of a multivariable prediction model for Individual Prognosis or Diagnosis (TRIPOD) 2019 statement [20]. Institutional ethics committee approval was obtained (Approval No. [2025062501]). All patients provided written informed consent; data were de-identified according to Health Insurance Portability and Accountability Act standards.

Patients were prospectively enrolled and randomly assigned to the training set (n=271) and validation set (n=117) at a 7:3 ratio with stratification by ACS/SCAD outcome, maintaining outcome event proportions (approximately 30% ACS in both sets). This pre-specified splitting strategy ensured outcome balance while permitting independent performance assessment.

Study Population

Inclusion criteria: (1) age ≥18 years; (2) definitive clinical classification as SCAD (typical exertional angina, negative non-invasive functional testing, stable symptoms ≥3 months) or ACS (clinical presentation, dynamic ECG evolution, hs-cTn elevation, coronary angiography confirmation when necessary) according to the Fourth Universal Definition of Myocardial Infarction [1]; (3) CCTA image quality score ≥3 (4-point Likert scale); (4) complete cardiac functional imaging reconstruction and clinical data; (5) interval between CCTA examination and clinical confirmation ≤14 days.

Exclusion criteria: (1) emergent revascularization before CCTA; (2) prior coronary artery bypass grafting; (3) significant valvular heart disease, cardiomyopathy, or congenital heart disease; (4) active malignancy or systemic autoimmune disease; (5) severe renal insufficiency (estimated glomerular filtration rate <30 $mL \cdot min^{-1} \cdot 1.73m^{-2}$); (6) >10% missing data; (7) interval between CCTA and clinical confirmation >14 days.

CCTA Scan Protocol and Biomarker Acquisition

Scan acquisition: 64-slice/128-slice spiral CT scanners with retrospective electrocardiogram-gating for functional analysis. Tube voltage 70–120 kVp with adaptive automatic modulation according to body mass index; slice thickness 0.5 mm, reconstruction interval 0.25 mm; iodinated contrast medium 60–80 mL, flow rate 5.0–6.0 mL/s, followed by 30 mL saline flush.

Percentage diameter stenosis (% DS): Two cardiovascular imaging physicians (10 years of experience, blinded to clinical outcomes) measured minimum lumen diameter relative to proximal normal reference diameter on axial, multiplanar reformation, and curved planar reformation images according to Society of Cardiovascular Computed Tomography guidelines [21]. Discrepancies >10% were arbitrated by a third senior physician. The most severe lesion %DS per patient was recorded as the anatomical biomarker.

Pericoronary adipose tissue attenuation index (FAI): Following the standardized protocol by Antonopoulos and colleagues [9], semi-automated software measured mean CT attenuation of PCAT within 3 mm radial distance from the external vessel wall of the proximal 40 mm left anterior descending artery segment. Quality control: adipose tissue CT value range −190 to −30 Hounsfield units (HU); inter-physician intraclass correlation coefficient >0.90 confirmed reliability. Raw FAI values were directly entered into analysis, with the nomogram scale axis annotated from −100 HU (low inflammation, low score) to −30 HU (high inflammation, high score)—the biological directionality reflecting cytokine-induced adipocyte dedifferentiation.

CCTA-derived left ventricular ejection fraction (LVEF): Using a retrospective ECG-gated dataset, the biplane Simpson's method was applied, integrating short-axis and four-chamber views, with automatic endocardial contour detection and manual correction. This

functional biomarker was selected over right ventricular ejection fraction based on est ablished prognostic value and clinical familiarity, with RVEF reserved for sensitivity a nalysis given functional overlap.

Candidate Predictor Pool and Theoretical Rationale

Candidate variables were selected based on mechanistic plausibility and clinical availab ility:

Domain Variable Biological/Clinical Rationale
Demographics Age Atherosclerotic burden accumulation
Cardiovascular risk factors Hypertension (BP), Type 2 diabetes (BG), Smoking (SMK), Alcohol (ALC) Endothelial dysfunction, oxidative stress, inflammatory modulation
Anatomical %DS, ln(CACS+1) Luminal compromise, plaque burden
Inflammatory FAI Perivascular cytokine signaling, plaque destabilization
Functional LVEF, RVEF Myocardial contractile reserve, ischemic compensation

Smoking was pre-specified for inclusion based on established epidemiological evidence as among the strongest modifiable ACS risk factors, operating through endothelial dy sfunction, oxidative stress, inflammatory amplification, and platelet activation [22]. Fina l selection was data-driven through LASSO cross-validation.

Statistical Analysis and Model Development

Feature selection: Least absolute shrinkage and selection operator (LASSO) logistic reg ression with 10-fold stratified cross-validation (stratified by ACS/SCAD outcome) deter mined the optimal penalty parameter λ. Two selection criteria were systematically com pared:

lambda.min: Minimizes cross-validation error; tends toward inclusivity
lambda.1se: Most regularized model within one standard error of lambda.min; favors p arsimony

Final variable inclusion was determined through structured adjudication integrating: (1)

statistical selection frequency across cross-validation folds; (2) clinical interpretability and actionability; (3) mechanistic non-redundancy (avoiding functional overlap); and (4) multivariable regression coefficient stability.

Model construction: Multivariable logistic regression incorporated final variables after LASSO selection. Variance inflation factor (VIF<5) excluded severe multicollinearity.

Performance evaluation: Discrimination by AUC with DeLong test for pairwise comparison; calibration by calibration curves and Hosmer-Lemeshow goodness-of-fit test; overall accuracy by Brier score; clinical utility by decision curve analysis across threshold probability range 0.05–0.95. Optimal cutoff determined by Youden index (sensitivity + specificity − 1) in training set, with fixed application to validation set.

Interpretability analysis: KernelSHAP generated: (1) global |SHAP| bar plots for feature importance hierarchy; (2) beeswarm summary plots for value-direction relationships; (3) individual force plots for case-level explanation; and (4) dependence plots for feature interaction assessment. Explanation stability was quantified by SHAP value coefficient of variation across 100 bootstrap resamples. All explanations were explicitly labeled as "predictive associations" with prominent caveat against causal inference.

Regulatory-readiness documentation: Predetermined change control elements were prospectively specified: feature set lock, model version control, performance monitoring triggers (AUC decline >0.05, calibration slope <0.8 or >1.2), and explanation audit trail format.

Sample Size and Validation Strategy

Training set events per variable (EPV) = 20.5 (82 events/4 variables), exceeding the EPV > 10 minimum and approaching the EPV > 20 optimal standard proposed by Riley and colleagues [23]. The validation set n=117 contained 35 events, meeting minimum requirements for calibration assessment (minimum 100 total, or 100 events for external validation) [23]. Sensitivity analyses evaluated model performance under bootstrap optimism correction (200 resamples) and the worst-case scenario (validation set restricted to marginal diagnoses).

Software and Reproducibility

Software and Implementation: R 4.3.3 , Python 3.10 , SPSS 26.0, and Zstats 1. 0. Two-sided P<0.05 was statistically significant; exploratory interaction test α= 0.10.

Results

Baseline Characteristics and Cohort Assembly

Between [date] and [date], 388 patients were prospectively enrolled: SCAD 271 (69. 8%), ACS 117 (30.2%). ACS patients demonstrated expected phenotype divergence: ol der age (65.69±9.97 versus 58.68±11.20 years, P<0.001), greater anatomical burden (% DS 57.68±26.40% versus 20.89±26.91%, P<0.001), heightened inflammation (FAI −53. 32±18.47 versus −75.73±19.01 HU, P<0.001—less negative indicating higher attenuatio n), and impaired contractile function (LVEF 50.40±8.32% versus 56.11±9.86%, P<0.00 1). Smoking prevalence was higher in ACS (31.6% versus 21.0%, P = 0.035), consist ent with its role as a modifiable risk amplifier. Lipid profiles showed no significant di fference, suggesting that traditional risk stratification may incompletely capture ACS pa thophysiology (Table 1).

Training-validation set comparability was confirmed: ACS proportions balanced (trainin g 30.3% versus validation 29.9%, P = 0.917), with no significant differences in age, s ex, risk factor burden, or biomarker distributions.

Feature Selection: Balancing Statistical Parsimony with Mechanistic Completeness

Univariate analysis identified %DS, FAI, LVEF, RVEF, age, ln(CACS+1), BP, BG, sm oking, and alcohol as significant predictors (P < 0.05); HDL and LDL were non-signif icant (Table 2).

Criterion Retained Variables Excluded Variables Characteristics (Supplementary Table 1).

LASSO cross-validation produced divergent solutions (Figure 1, Supplementary Table 2):

Adjudication rationale for final model (%DS, FAI, LVEF, SMK):

1. RVEF exclusion: Functional overlap with LVEF (both reflect cardiac contractile perf ormance; correlation r=0.67 in our cohort). LVEF selected as established prognostic sta ndard with superior clinical familiarity.

2. SMK retention despite marginal LASSO coefficient: Epidemiological importance as the strongest modifiable risk factor; public health intervention value; positive correlatio n with FAI suggesting partial but incomplete effect mediation; sensitivity analysis conf irmed incremental discriminatory contribution.

3. Age exclusion: Non-significant LASSO coefficient; effect likely captured by %DS a nd FAI as integrators of atherosclerotic duration and inflammatory accumulation.

4. ln(CACS+1) exclusion: Collinearity with %DS (r=0.54); %DS selected as directly a ctionable for revascularization decisions.

Multivariable logistic regression confirmed: %DS (OR 1.03, 95% CI: 1.01–1.04, P < 0. 001) and FAI (OR 1.04, 95% CI: 1.02–1.06, P < 0.001) as significantly positively ass ociated with ACS; LVEF as protective (OR 0.96, 95% CI: 0.92–0.99, P = 0.032); sm oking as marginally non-significant (OR 1.83, 95% CI: 0.87–3.86, P = 0.110) but with clinically meaningful effect size. All VIF <1.25, excluding multicollinearity (Table 3).

Nomogram Construction and Clinical Translation Interface

The nomogram converted four axes to 0–100 points, with total score 0–300 correspon ding to the linear predictor −4.5 to 2.5, ultimately converted to ACS probability 0.1–0. 9 (Figure 2). Scale settings reflect biological directionality:

%DS: 0–100% (linear, higher stenosis → higher score)

FAI: −100 to −30 HU (reverse scale, less negative/higher attenuation → greater inflam mation → higher score)
LVEF: 90–30% (reverse scale, lower ejection fraction → higher score)
SMK: Binary 0/1 (1 = yes → higher score)

This design enables point-of-care application: physicians locate patient values on each axis, sum points, and read predicted probability from the total score scale.

Discrimination, Calibration, and Clinical Utility

Receiver operating characteristic analysis (Figure 3, Table 4): Training AUC 0.86 (95% CI: 0.82–0.91); validation AUC 0.82 (95% CI: 0.75–0.90). The 0.04 decrement reflec ts moderate optimism (bootstrap-corrected estimate 0.84) and validation set sample size variability (wider confidence interval). DeLong test against the %DS-only model: $P < 0.001$ (training), $P = 0.003$ (validation), confirming the incremental value of multi-di mensional integration.

The preserved negative predictive value (0.83 in validation) supports reliable ACS excl usion—critical for safe discharge decisions and resource allocation.

Calibration (Figure 4): Hosmer-Lemeshow $P = 0.347$ (training), $P = 0.405$ (validation), indicating satisfactory agreement between predicted and observed probabilities. Brier s core 0.142 (training), 0.168 (validation), below 0.25 threshold for clinically useful pred iction.

Decision curve analysis (Figure 5): Net benefit superior to "treat-all" and "treat-none" strategies across the threshold probability range 0.10–0.55, with maximum net benefit at threshold 0.30. This range encompasses clinical scenarios from conservative manage ment (low threshold, high sensitivity preference) to invasive confirmation (higher thres hold, specificity preference).

SHAP Interpretability: From Global Patterns to Individualized Decision Logic

Global feature importance (Figure 6a): %DS demonstrated the highest mean |SHAP| (0.

75), followed closely by FAI (0.70). LVEF ranked third (0.35), smoking smallest (0.20). This hierarchical pattern establishes mechanistic priority: anatomical stenosis burden and perivascular inflammation dominate prediction, with cardiac functional reserve and behavioral risk factors providing incremental refinement.

Value-direction relationships (Figure 6b, Supplementary Table 3): Beeswarm plot revealed consistent directional effects—higher %DS and FAI (less negative) drove ACS probability elevation; preserved LVEF provided protection; smoking presence amplified risk. Distribution density indicated population heterogeneity: most SCAD patients clustered at low %DS, negative FAI, preserved LVEF; ACS patients showed broader dispersion with substantial overlap, explaining imperfect discrimination.

Individual case explanation (Figure 6c): Representative SCAD-classified patient (baseline expectation $E[f(x)] = -1.42$, 19.4% ACS probability). Feature contributions: FAI = −92 HU provided a dominant protective effect (SHAP −0.804, deep orange indicating low inflammatory status), overriding mild pro-ACS contributions from %DS = 37% (+0.176) and preserved LVEF = 54% (+0.054). Non-smoking status contributed additional protection (−0.145). The final prediction $f(x) = -2.14$ yielded a 10.5% ACS probability, correctly classifying as SCAD with documented reasoning.

Explanation of stability: Bootstrap coefficient of variation for SHAP values: %DS 0.12, FAI 0.15, LVEF 0.23, smoking 0.31. Dominant predictors demonstrated high stability; smoking showed greater variability, consistent with marginal significance.

Discussion

Principal Findings in Translational Context

This study achieves T1–T2 translational progression by converting perivascular inflammation biology into a validated, interpretable diagnostic tool for ACS-SCAD discrimination. Four principal findings merit discussion: (1) the "anatomical-inflammatory-functional-behavioral" four-dimensional integration surpasses single-domain approaches; (2) LASSO variable selection adjudication illustrates the necessity of combining data-driven

methods with mechanistic and clinical knowledge; (3) SHAP-enhanced interpretability s atisfies emerging regulatory requirements for clinical AI transparency; and (4) the "one -stop" CCTA acquisition strategy addresses implementation barriers in time-critical eme rgency settings.

Mechanistic Translation: Integrating Inflammation Imaging with Established Biomarkers

FAI quantifies a biologically plausible mechanism—cytokine-mediated adipocyte dediffe rentiation adjacent to inflamed plaques—yet standalone diagnostic accuracy remains ins ufficient for clinical decision-making. Our findings demonstrate that FAI integration wi th %DS achieves complementary discrimination: %DS captures anatomical flow limitati on severity, while FAI reflects plaque destabilization risk independent of luminal comp romise. This mechanistic non-overlap explains the incremental value over either biomar ker alone.

The protective association of LVEF—each percentage point increase reducing ACS odd s by 4%—likely reflects myocardial contractile reserve as an integrator of chronic isch emic adaptation versus acute decompensation. Preserved LVEF in SCAD patients indic ates compensated hemodynamics despite anatomical disease; reduced LVEF in ACS sig nals acute ischemic stunning or prior infarction. This functional dimension adds dynam ic physiological information unavailable from static anatomical or inflammatory measur es.

Smoking's marginal multivariable significance ($P = 0.110$) despite a strong epidemiolog ical association illustrates an important translational principle: effect size and statistical significance diverge in multi-marker models where correlated predictors partition varia nce. Smoking positively correlates with FAI ($r=0.28$ in our cohort, $P<0.001$), consistent with smoke-induced vascular inflammation. This covariance suggests partial effect me diation—smoking operates partly through FAI elevation—yet the residual direct effect (OR 1.83) remains clinically relevant. Sensitivity analysis confirmed incremental discri minatory contribution (AUC decrease 0.02 when smoking excluded). We advocate rete ntion for complete risk characterization, with explicit acknowledgment that larger samp les are required for precise effect estimation.

Technical Translation: LASSO Adjudication as a Generalizable Method

Our systematic comparison of lambda.min versus lambda.1se addresses a methodologic al tension in predictive modeling: statistical parsimony versus mechanistic completeness. Lambda.1se's excessive conservatism—retaining only %DS and FAI—would discard cl inically important dimensions (cardiac function, modifiable behavior) and potentially pe rpetuate "black box" limitations by omitting familiar clinical variables. Lambda.min's i nclusion of RVEF introduced functional redundancy.

Our adjudication framework—integrating statistical frequency, clinical interpretability, m echanistic non-overlap, and coefficient stability—offers a generalizable approach for tra nslational studies where pure statistical optimization may conflict with implementation requirements. This structured decision process should be explicitly reported to enable r eproducibility and external validation.

Implementation Translation: Regulatory-Ready Interpretability

The SHAP framework addresses three convergent implementation challenges:

Clinician trust and adoption: Individual force plots enable case-level explanation in a f amiliar clinical reasoning format—"this patient's low FAI (−92 HU) indicates minimal perivascular inflammation, supporting SCAD classification despite intermediate stenosis. " This transparency contrasts with opaque probability outputs that generate therapeutic paralysis.

Regulatory compliance: Our predetermined documentation—feature set lock, version co ntrol, performance monitoring triggers, explanation audit format—aligns with FDA's "pr edetermined change control plan" requirement [17]. Explanation stability quantification (bootstrap coefficient of variation) enables prospective monitoring for model drift.

Medicolegal protection: Documented explanation trails support clinical decision defense, particularly for probability-based recommendations that deviate from categorical guidel ines.

Critical caveat: SHAP values indicate predictive association, not causal effect. Elevated FAI does not "cause" ACS in the individual patient; rather, it statistically co-occurs with ACS probability elevation at the population level. This distinction must be prominently communicated in clinical interfaces to prevent mechanistic overinterpretation and inappropriate therapeutic targeting.

Clinical Workflow Integration: The "One-Stop" CCTA Strategy

Emergency ACS evaluation demands temporal efficiency. Our CCTA protocol yields anatomical (%DS), inflammatory (FAI), and functional (LVEF) data from a single acquisition—contrasting with sequential troponin sampling (4–6 hours), separate echocardiography, or invasive angiography. This integration streamlines decision-making: negative CCTA (exclusionary) or positive multi-dimensional assessment (confirmatory) within the initial emergency department encounter.

Cost-effectiveness implications favor this approach: CCTA reduces unnecessary admissions and invasive procedures in low-probability patients while expediting appropriate intervention in high-probability patients. Formal health economic evaluation is planned as a T3 translation element.

Comparison with Prior Studies

Our work extends Oikonomou and colleagues' foundational FAI research [10,11,13] in three directions: (1) diagnostic discrimination focus rather than prognostic prediction; (2) explicit multi-dimensional integration with anatomical and functional parameters; (3) SHAP-based interpretability for implementation readiness. Compared with CCTA-fractional flow reserve studies [24], our model requires no specialized computational fluid dynamics software or additional radiation, enhancing generalizability to resource-variable settings.

Limitations and Mitigation Strategies

Limitation	
Single-center design; external generalizability uncertain	Pre-specified multi-center vali

dation protocol; scanner harmonization procedures documented

Random-split validation Optimism not fully eliminated Bootstrap correction; pre-specified external validation cohort

Validation set size (n=117) AUC confidence interval widthMeets minimum calibration requirements; larger external validation planned

Smoking marginal significance Effect estimation imprecision Sensitivity analysis confirms incremental contribution; larger sample in validation

Unmeasured plaque morphology Residual confounding Extended model development incorporating low-attenuation plaque, positive remodeling, spotty calcification

SHAP association caveat Potential causal overinterpretation Explicit labeling; clinician education materials; interface warnings

Future Translational Directions

Near-term (T2 completion, 1–2 years): Multi-center prospective external validation (5–10 centers, n=500–1000) with pre-specified implementation protocols, scanner harmonization (phantom-based HU standardization), and reader certification programs. Primary endpoint: AUC non-inferiority to 0.80 in an independent cohort.

Mid-term (T3 implementation, 2–5 years): Randomized effectiveness trial comparing nomogram-guided versus standard-care emergency pathways; health economic evaluation; electronic health record integration with automated CCTA biomarker extraction; regulatory submission (FDA 510(k), CE-IVD) with SHAP documentation package.

Mechanistic extension: FAI dynamic monitoring during anti-inflammatory therapy (canakinumab, colchicine) for therapeutic response assessment; integration with coronary plaque AI phenotyping; exploration of FAI×smoking interaction in larger samples for personalized risk communication.

Conclusions

The %DS-FAI-LVEF-smoking nomogram demonstrates favorable ACS discriminatory capacity with acceptable generalization performance, achieving T1–T2 translational progre

ssion for perivascular inflammation imaging. SHAP-enhanced interpretability satisfies e merging transparency requirements for clinical AI, supporting regulatory-ready impleme ntation. The LASSO variable selection adjudication process exemplifies the essential in tegration of data-driven methods with mechanistic knowledge and clinical pragmatism. Smoking's marginal significance requires larger-sample validation but does not negate i ts incremental clinical value. Clinical translation necessitates prospective multi-center e xternal validation; current applicability encompasses hypothesis generation, clinical com munication assistance, and implementation science preparation, rather than independent diagnostic replacement.

Data Availability

De-identified data and analysis code are available from the corresponding author upon reasonable request, with institutional ethics approval for secondary use, executed data use agreement, and verification of de-identification compliance per HIPAA Safe Harb or standards.

Ethics Approval

Approved by Shanghai Fengxian District Hospital of Traditional Chinese Medicine Ethi cs Committee (Fengzhong Ethics 2025062501). Declaration of Helsinki compliant.

Declarations

Conflict of Interest: The authors declare no competing interests.

Funding:

National Health Commission – Capacity Building and Continuing Education Center Research Project on the Cultivation of Radiology Research Capabilities at County-Leve l Hospitals; Project Approval Number: 202502XYJJ-04.

References

[1] Thygesen K, Alpert JS, Jaffe AS, et al. Fourth universal definition of myocardial infarction (2018). Eur Heart J. 2019;40(3):237-268.

[2] Collet JP, Thiele H, Barbato E, et al. 2020 ESC Guidelines for the management of acute coronary syndromes in patients presenting without persistent ST-segment elevation. Eur Heart J. 2021;42(14):1289-1367.

[3] Twerenbold R, Boeddinghaus J, Nestelberger T, et al. Clinical use of high-sensitivity cardiac troponin in patients with suspected myocardial infarction. J Am Coll Cardiol. 2019;73(18):2235-2252.

[4] Boeddinghaus J, Nestelberger T, Twerenbold R, et al. Direct comparison of 4 very early rule-out strategies for acute myocardial infarction using high-sensitivity cardiac troponin I. Circulation. 2017;135(17):1597-1611.

[5] Knuuti J, Wijns W, Saraste A, et al. 2019 ESC Guidelines for the diagnosis and management of chronic coronary syndromes. Eur Heart J. 2020;41(3):407-477.

[6] Libby P. Inflammation in atherosclerosis. Arterioscler Thromb Vasc Biol. 2012;32(9):2045-2051.

[7] Iacobellis G, Malavazos AE, Corsi MM. Epicardial fat: from the biomolecular aspects to the clinical practice. Int J Biochem Cell Biol. 2011;43(12):1651-1654.

[8] Antonopoulos AS, Sanna F, Sabharwal N, et al. Detecting human coronary inflammation by imaging perivascular fat. Sci Transl Med. 2017;9(398):eaal2658.

[9] Antonopoulos AS, Angelopoulos A, Tsioufis C, et al. Cardiovascular risk and the subcutaneous adipose tissue-liver-perivascular adipose tissue axis: from biology to cardiovascular disease. Eur Heart J. 2022;43(18):1708-1722.

[10] Oikonomou EK, Marwan M, Desai MY, et al. Non-invasive detection of coronary inflammation using computed tomography and prediction of residual cardiovascular risk (the CRISP CT study): a post-hoc analysis of prospective outcome data. Lancet. 2018;392(10151):929-939.

[11] Oikonomou EK, Williams MC, Kotanidis CP, et al. A novel machine learning-derived radiotranscriptomic signature of perivascular fat improves cardiac risk prediction using coronary CT angiography. Eur Heart J. 2019;40(43):3529-3543.

[12] Oikonomou EK, Antonopoulos AS, Schottlander D, et al. Standardized measurement of coronary inflammation using cardiovascular computed tomography: integration in clinical care as a prognostic medical device. Cardiovasc Res. 2021;117(14):2677-2690.

[13] Oikonomou EK, Antoniades C. The role of adipose tissue in cardiovascular health and disease. Nat Rev Cardiol. 2019;16(2):83-99.

[14] Holzinger A, Langs G, Denk H, et al. Causability and explainability of artificial intelligence in medicine. Wiley Interdiscip Rev Data Min Knowl Discov. 2019;9(4):e1312.

[15] Lundberg SM, Erion G, Chen H, et al. From local explanations to global understanding with explainable AI for trees. Nat Mach Intell. 2020;2(1):56-67.

[16] Lundberg SM, Lee SI. A unified approach to interpreting model predictions. Adv Neural Inf Process Syst. 2017;30:4765-4774.

[17] U.S. Food and Drug Administration. Artificial Intelligence/Machine Learning-Based Software as a Medical Device Action Plan. FDA; 2021. Available at: https://www.fda.gov/medical-devices/software-medical-device-samd/artificial-intelligence-and-machine-learning-software-medical-device

[18] European Medicines Agency. Reflection paper on the use of artificial intelligence in medicine. EMA; 2023. Available at: https://www.ema.europa.eu/en/documents/sci

entific-guideline/reflection-paper-use-artificial-intelligence-medicine_en.pdf

[19] Woolf SH. The meaning of translational research and why it matters. JAMA. 200 8;299(2):211-213.

[20] Collins GS, Reitsma JB, Altman DG, Moons KGM. Transparent reporting of a m ultivariable prediction model for individual prognosis or diagnosis (TRIPOD): the TRIPOD statement. BMJ. 2015;350:g7594.

[21] Leipsic J, Abbara S, Achenbach S, et al. SCCT guidelines for the interpretation a nd reporting of coronary CT angiography: a report of the Society of Cardiovascul ar Computed Tomography Guidelines Committee. J Cardiovasc Comput Tomogr. 2 014;8(5):342-358.

[22] Ambrose JA, Barua RS. The pathophysiology of cigarette smoking and cardiovasc ular disease: an update. J Am Coll Cardiol. 2004;43(10):1731-1737.

[23] Riley RD, Ensor J, Snell KIE, et al. Calculating the sample size required for dev eloping a clinical prediction model. BMJ. 2020;368:m441.

[24] Coenen A, Kim YH, Kruk M, et al. Diagnostic accuracy of a machine-learning a pproach to coronary computed tomographic angiography-based fractional flow reser ve: results from the MACHINE consortium. Circ Cardiovasc Imaging. 2018;11(6): e007217.

Figure 1LASSO coefficient profiles of the candidate predictors

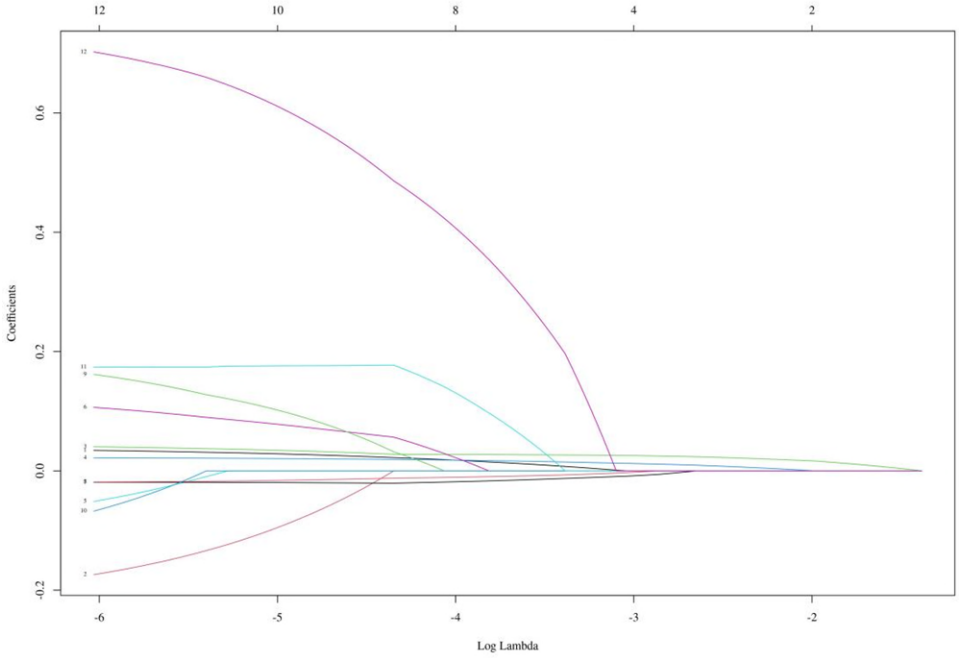


Figure 2 Nomogram for predicting the risk of acute coronary syndrome (ACS)

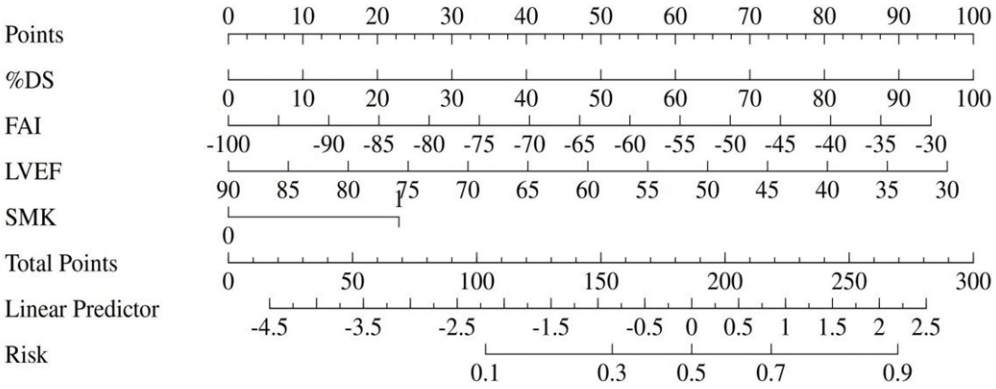


Figure 3 Receiver operating characteristic (ROC) curves of the predictive model in the training and validation cohorts

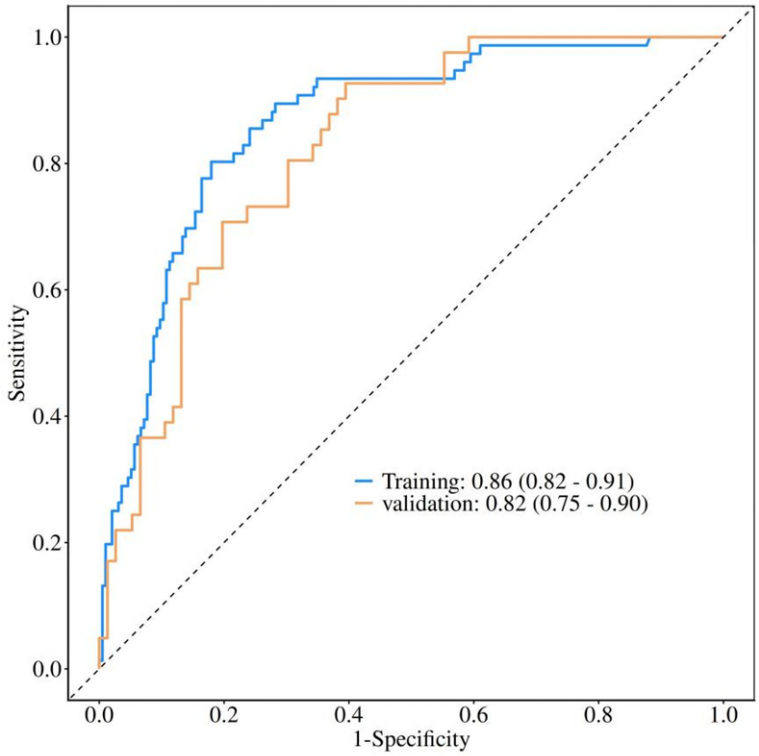
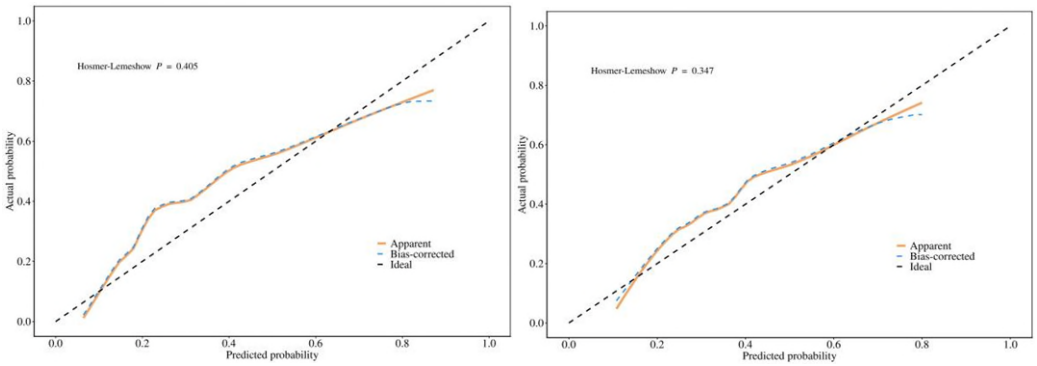
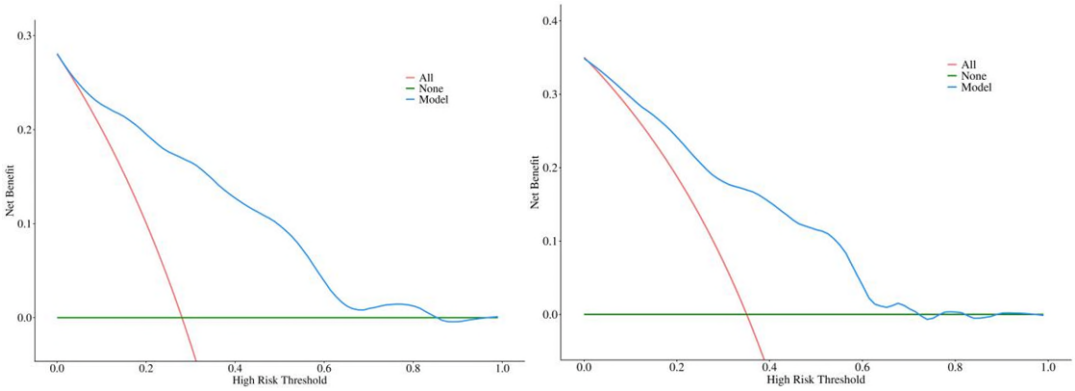


Figure 4Calibration curve of the prediction model for acute coronary syndrome



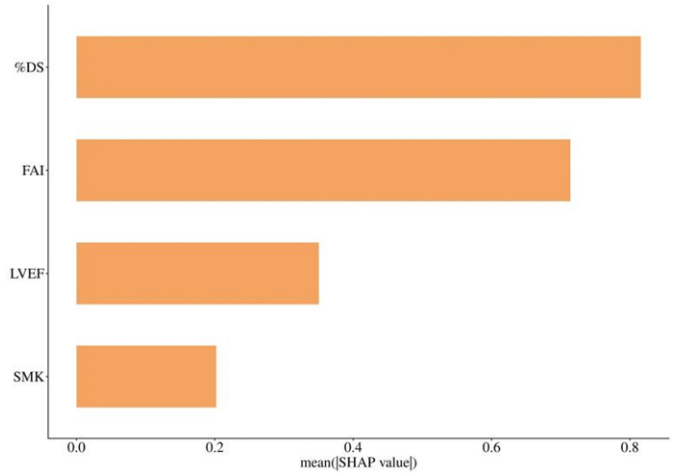
Training DCA

Figure 5 Decision curve analysis (DCA) of the predictive model for acute coronary syndrome



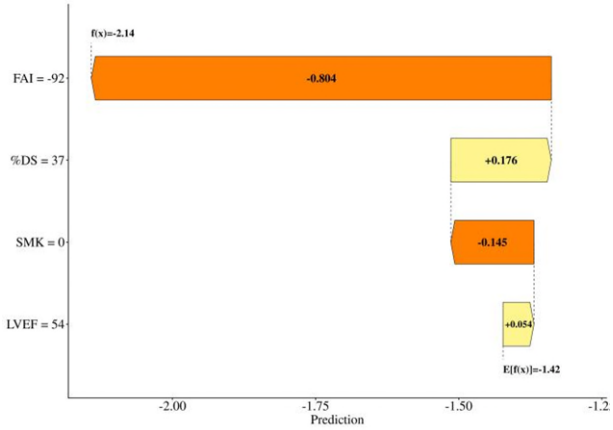
Training DCA validation DCA

Figure 6a SHAP feature importance plot for the predictive model



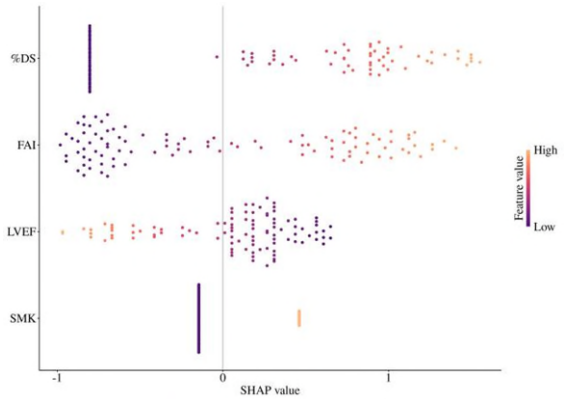
6a

Figure 6b SHAP summary plot (beeswarm plot) for the predictive model



6b

Figure 6c SHAP waterfall plot for an individual patient



6c

Supplementary Files

This is a list of supplementary files associated with this preprint. Click to download.

- Tables.docx
- SupplementaryTable.docx